



# Vegetation canopy cover effects on sediment erosion processes in the Upper Colorado River Basin Mancos Shale formation, Price, Utah, USA



Erik M. Cadaret<sup>a</sup>, Kenneth C. McGwire<sup>a,\*</sup>, Sayjro K. Nouwakpo<sup>b</sup>, Mark A. Weltz<sup>c</sup>, Laurel Saito<sup>b</sup>

<sup>a</sup> Desert Research Institute, Division of Earth and Ecosystem Sciences, Reno, NV, USA

<sup>b</sup> University of Nevada Reno, Department of Natural Resources and Environmental Science, Reno, NV, USA

<sup>c</sup> U.S. Department of Agriculture, Agricultural Research Service, Great Basin Rangelands Research Unit, Reno, NV, USA

## ARTICLE INFO

### Article history:

Received 12 February 2016

Received in revised form 30 April 2016

Accepted 29 June 2016

Available online xxxx

### Keywords:

Saline soils

Rangeland Hydrology Erosion Model

Calibration

Vegetation-driven spatial heterogeneity

Landscape metrics

Price River

## ABSTRACT

This study investigated erosion processes on the highly erosive, saline soils of the Mancos Shale formation in the Price-San Rafael River Basin in Utah, USA. Rainfall simulations were performed at two sites using a Walnut Gulch rainfall simulator with a variety of slope angles and rainfall intensities. The Rangeland Hydrology Erosion Model (RHEM) was calibrated to provide unbiased estimates of discharge and sediment load in runoff at each site. RHEM simulated the inter-plot variability best at the site with higher slope angles, vegetation cover, and sediment loads. The calibrated surface erosion parameters in RHEM ( $K_{ss}$ ,  $K_{\omega}$ ) were substantially greater than any published in prior studies from non-saline environments. The spatial distribution of vegetation canopy cover was quantified using photogrammetric modeling and landscape pattern metrics. As the patches of vegetation became more contiguous and the tortuosity of the bare soil area increased, RHEM over-predicted sediment output, suggesting that vegetation-driven spatial heterogeneity influenced erosion in a way that is not captured by the model.

© 2016 Elsevier B.V. All rights reserved.

## 1. Introduction

The Colorado River Basin is a primary source of water for seven states in the western United States and the Baja region of Mexico. The U.S. Bureau of Reclamation predicts that climate change, increasing water demand, and water scarcity will exacerbate the current salinity challenges of the Colorado River (USBOR, 2005). The Mancos Shale geological formation spans a wide area in the Upper Colorado River Basin, and its severely eroding rangelands have been identified as a major producer of sediment, salinity, and selenium to the Colorado River (Evangelou et al., 1984; Tuttle et al., 2014a, 2014b). Rasely et al. (1991) estimate that 7–15% of the rangeland areas in the state of Utah (USA) are in a severely eroding condition and are responsible for 75–90% of the increasing sediment and salt yields. Two field sites that represent severely eroding conditions on the Mancos Shale formation were selected for study within the Price and San Rafael River basins in the state of Utah. The Price River contributes <1% of the water to the

Colorado River, but approximately 3% of the salt load (Rao et al., 1984). These field sites were located on different members of the formation, providing some insight into the variability of erosion processes within the Mancos Shale. Rainfall simulations were performed to calibrate the Rangeland Hydrology and Erosion Model (RHEM; Nearing et al., 2011) in order to determine what parameter values are required for the erodible saline soils of the Mancos Shale and to investigate how the amount and spatial distribution of vegetation cover may affect sediment loading.

The RHEM simulates hillslope runoff and erosion responses using two process-model components. The hydrology component of the RHEM is based on the KINEROS2 model that incorporates rainfall interception by vegetation, infiltration and overland flow (Smith et al., 1995). The erosion component of RHEM incorporates concentrated flow (Foster, 1982) and splash and sheet flow (Wei et al., 2009) to simulate soil erosion (Al-Hamdan et al., 2015). The current version of RHEM (v2.3) models splash/sheet erosion as the primary driver of erosion, while concentrated flow transports the eroded sediments (M. Hernandez, USDA, pers. comm. 2015). A number of prior studies have successfully used RHEM to model erosion (Al-Hamdan et al., 2012, 2015; Felegari et al., 2014; Hernandez et al., 2013; Zhang et al., 2012; Nearing et al., 2011), but none of these have been performed on the types of saline and sodic soils found in the Mancos Shale formation.

Vegetation canopy cover (VCC) intercepts raindrop impact and reduces runoff by promoting infiltration (Wischmeier and Smith, 1978; Loch, 2000; Branson et al., 1981). Wood et al. (1998) found that at the

*Abbreviations:* RHEM, Rangeland Hydrology Erosion Model; VCC, Vegetation canopy cover; VDSH, Vegetation-driven spatial heterogeneity; WGRS, Walnut Gulch rainfall simulator; SFM, Structure from motion; MOCOM, Multi-objective complex optimization method; NSE, Nash-Sutcliffe efficiency; RSR, Ratio of root-mean-squared error to standard deviation; FRAC\_CV, Coefficient of variation for fractal dimension metric; CONTIG\_CV, Coefficient of variation for contiguity index metric.

\* Corresponding author at: Desert Research Institute, Division of Earth and Ecosystem Sciences, 2215 Raggio Parkway, Reno, NV 89512, USA.

E-mail address: [kenm@dri.edu](mailto:kenm@dri.edu) (K.C. McGwire).

beginning of a rainfall event, canopies efficiently intercept rainfall within their projected area, until the maximum cumulative interception threshold is exceeded. The amount of time to reach maximum cumulative interception is dependent upon the type of plant and the rainfall intensity (Wood et al., 1998). Proportionally, rainfall lost to vegetation interception is most prominent under conditions of lower rainfall intensities and may strongly influence erosion rates under such conditions (Simanton et al., 1991). Carroll et al. (2000) found that as VCC increases on varying slopes, there is a reduction in runoff electrical conductivity (EC) and sediment loss, and therefore concluded that successful establishment of VCC is an effective way to improve water quality. Bartley et al. (2006) found that even with high mean VCC, small interspaces of bare soil had six to nine times more runoff and 60 times more sediment loss than similar hillslopes that did not contain as much or any interspace patches. In addition, the majority of the sediment load from the hillslopes measured by Bartley et al. consisted of fine suspended load rather than coarse bedload material and the majority of soil loss occurred during the initial runoff event. Bartley et al. (2006) also highlight the importance of having medium to high vegetation cover at the bottom of hillslopes to trap and store sediment.

The distribution of vegetation and interspace areas leads to vegetation-driven spatial heterogeneity (VDSH) in soil development and evolution processes (Puigdefabregas, 2005) that influence sheet runoff and concentrated flow processes. This in turn influences rill and channel development and thereby affects sediment loading along those flow paths (Wilcox et al., 1996; Davenport et al., 1998; Urgeghe et al., 2010). Since the capacity for heterogeneity is constrained when vegetation cover is very low or very high, VDSH is not independent of VCC. If vegetation is sparse and there is little complexity to the pattern of obstacles, runoff tends to concentrate in narrow channels (Al-Hamdan et al., 2012). At moderate levels of vegetation cover, a simple pattern of cover might also concentrate flow while complex cover might interrupt flow and widen channels. This differential response would reflect the existence of a channel network characterized by VDSH (Puigdefabregas, 2005). VDSH may also affect the amount of infiltration (Chartier et al., 2011), soil nutrients, and trapped sediment (Zucca et al., 2011; Howes and

Abrahams, 2003). We hypothesize that VDSH may have an effect on sediment erosion processes that is not currently parameterized and therefore not captured by the RHEM.

## 2. Material and methods

### 2.1. Site description and plot installation

The study area is located near Price, Utah in the Price-San Rafael River basin ( $1.1 \times 10^4 \text{ km}^2$ ). This is a sparsely populated area within the Colorado Plateau that is characterized by an uplifted, eroded, and deeply dissected tableland that contains a salt-desert shrubland ecosystem. The annual mean precipitation at Price is  $227 \text{ mm yr}^{-1}$  (November =  $13.0 \text{ mm}$ , September =  $29.2 \text{ mm}$ ), and the annual mean air temperature is  $8.2 \text{ }^\circ\text{C}$  (January =  $-15.6 \text{ }^\circ\text{C}$ , July =  $32.7 \text{ }^\circ\text{C}$ ). Runoff is primarily from spring snowmelt and high intensity, short duration convective storms during the summer. The two field sites, named Price and Ferron, were selected for their location on the Mancos Shale formation, varying vegetation cover and slope, accessibility for field operations, and National Environmental Policy Act clearance. The Price site ( $110^\circ 36' 26'' \text{ W}$ ,  $39^\circ 27' 47'' \text{ N}$ ) is located within the Tununk member of the Mancos Shale formation, 23 km southeast of the city of Price at an elevation of 1700 MASL. The Ferron site ( $111^\circ 7' 21'' \text{ W}$ ,  $38^\circ 58' 23'' \text{ N}$ ) is located within the Blue Gate member of the Mancos Shale, 74 km south-southwest of Price at an elevation of 1900 MASL (Fig. 1).

The Price field site (Fig. 2A) contains well developed, light gray soil crusts on shallow slopes (0.6%–10%) with sparse vegetation cover (3.3%–17.8%). The soil series found at Price is the Persayo loam (USDA – NRCS, 2013a). The salt-tolerant vegetation includes a mixture of four shrubs (*Krascheninnikovia lanata*, *Chrysothamnus nauseosus*, *Atriplex gardneri*, *Ephedra viridis*), two subshrubs (*Eriogonum microthecum*, *Helianthella microcephala*), and three grass species (*Achnatherum hymenoides*, *Hilaria jamesii*, *Elymus elymoides*). The predominant plant species are *Ephedra viridis*, *Atriplex gardneri*, and *Achnatherum hymenoides*. The Ferron field site (Fig. 2B) contains poorly developed, light-medium gray soil crusts on steep slopes (11.4%–24.5%)

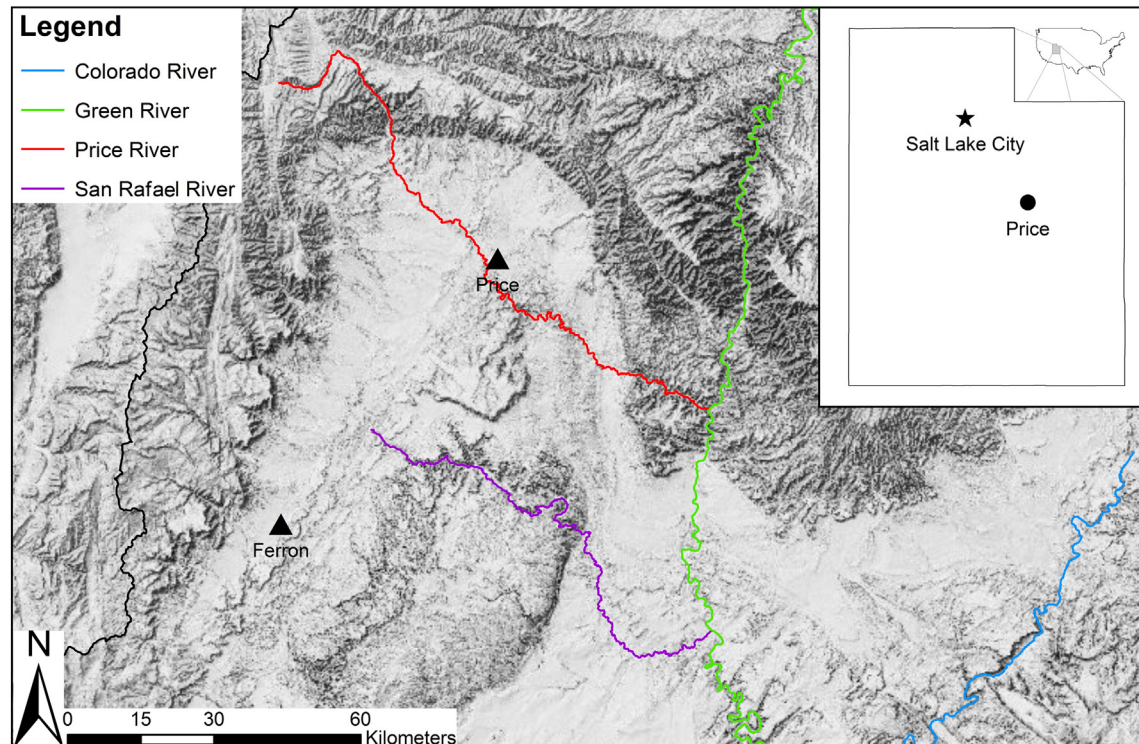


Fig. 1. Map of the field sites relative to rivers in the Upper Colorado River Basin, Utah, USA.



Fig. 2. Photographs of site conditions at Price (A) and Ferron (B).

with moderate vegetation cover (17.7%–25.2%). The soil series found at Ferron is the Chipeta-Badland complex (USDA – NRCS, 2013b). Patches of salt efflorescence are abundant at Ferron and the vegetation is solely comprised of the salt-tolerant shrub species *Atriplex corrugata*. Historical grazing has occurred at both sites, as indicated by scattered cattle and antelope hoof impressions.

Twelve 6 m × 2 m rainfall simulation plots were installed at each field site, allowing three replicates of four rainfall intensities: 2 year storms (50.8 mm h<sup>-1</sup>), 10 year storms (88.9 mm h<sup>-1</sup>), 25 year storms (114.3 mm h<sup>-1</sup>), and 50 year storms (139.7 mm h<sup>-1</sup>). Intensities were derived from 5 min rainfall amounts for the Price area from NOAA's Atlas14 database (<http://www.nws.noaa.gov/oh/hdsc/index.html>). The plots were aligned to existing flow paths that would keep concentrated flow off the rails at the edge of the plots. Each plot was used for a single rainfall simulation. Steel strips (2 m × 0.2 m) were installed along the top and side borders and a flume was installed flush with the soil at the bottom of the plot. Rainfall simulations used a version of the computer-controlled Walnut Gulch rainfall simulator (WGRS) (Paige et al., 2004) that completely and evenly covered the plot. Water for the simulator was transported by truck from the firehouse station at the Bureau of Land Management office in Price.

## 2.2. Field measurements

The slope of each plot was measured using a Nikon NPR 352 total station. Soils were sampled using a trowel at three locations under the vegetation canopy and at three bare soil locations. Soils at each location were separated into a surface sample and two subsurface samples (–5 cm and –10 cm). Soil texture was measured using the methods of Jackson and Barak (2005). Bulk density was calculated by measuring the dry weight of the collected samples and using the known volume of the 5 cm diameter by 3 cm long AMS soil sampler attachment. Porosity was determined by its relation to bulk density following Jury and Horton (2004).

Runoff sediment load samples were collected using 1 L Nalgene bottles. On the first field expedition to the Price site, ten rainfall simulations were completed in which runoff was collected following initiation of flow at the flume. Sampling was performed every 30 s for the first 9 min and then every minute thereafter over the 15-min simulation duration. On the second field expedition for two additional plots at Price and 12 plots at Ferron, the sampling protocol was changed because examination of hydrographs indicated that the first set of simulations did not run long enough for the discharge to consistently reach steady-state and there were insufficient resources to maintain the original sampling rate for a longer duration. On the second expedition, runoff was collected every 30 s for the first 3 min and then once every 3 min thereafter until discharge measured by the flume flow gauge reached equilibrium. A total of 263 runoff sediment load samples were collected with 133 samples from Price and 130 samples from Ferron.

## 2.3. Measuring vegetation canopy cover

The distribution of vegetation cover within each plot was mapped using high-resolution photogrammetric models that were calculated with Structure from Motion (SfM) three dimensional (3D) reconstruction using numerous handheld digital photographs (Nouwakpo et al., 2015). Individual 3D points were assessed to determine whether the points represented vegetation canopy versus soil or surface litter. A coarse estimation of soil surface topography was created by superimposing a 5 cm grid over the plot and finding the lowest 3D point within each grid cell. A second order polynomial trend surface was fit to these local minima, and points that were >20 cm above this trend surface were identified as tall vegetation based on field observations. For remaining points, two tests were applied. First, the slope from each point to each of its neighbors within 2.5 cm was calculated. The maximum slope within each of four directional quadrants was determined, and points were labeled as vegetation if the minimum value of the maximum slope from each quadrant was >20%. The strategy of using the minimum of maximum slope in each direction identified protrusions that were not part of the local trend in surface relief. For the second test, a height was interpolated for the location of each point using an inverse-distance weighting of its four nearest neighbors in each directional quadrant that had not yet been identified as vegetation. The point in question was labeled as vegetation if it was >2 cm above that interpolated height in order to minimize confusion between surface roughness and vegetation canopy.

Minor labeling errors occurred where sharp surface features were classified as vegetation, and these artifacts were manually edited. Irregularly sampled point clouds representing just vegetation were converted into a two dimensional map formed by superimposing a 2 mm grid and determining which grid cells contained a vegetation point. That fine grid was then aggregated to a 6 cm grid, and these coarser cells were labeled as canopy if more than half the fine-resolution grid cells nested within were labeled as having vegetation. This secondary aggregation helped reduce the effect of over-prediction from labeling a fine-resolution cell as majority-vegetation even if it had just one or two 3D samples within it. Basal, litter, and rock cover percentages were determined from 0.5-mm-resolution orthophotos of each plot.

The accuracy of the mapping method was tested by selecting a random plot (Price plot 5), and visually assessing 200 random test points that were split evenly between the areas labeled as vegetation and not-vegetation. Agreement between the automated method and the visual interpretation was 90%, with 8% commission error and 12% omission error for the vegetation.

## 2.4. Rangeland Hydrology Erosion Model

Background literature on the RHEM was reviewed to find which input parameters had well-defined reference values that were

**Table 1**  
Basic RHEM input parameters.

Input parameters	Description	Default values
CLEN	Hillslope length (m)	30
DIAMS	Soil particle diameters (mm)	0.002, 0.01, 0.03, 0.2, 0.3
DENSITY	Particle densities (g cm <sup>-3</sup> )	2.60, 2.65, 1.80, 1.60, 2.65
LEN	Plot slope length (m)	6
WIDTH	Plot slope width (m)	2
SX	Normalized distance	1
CV	Ke coefficient of variation	1
IN	Interception depth (mm)	1
G	Mean capillary drive (mm)	200
DIST	Pore size distribution	0.23
SMAX	Upper limit to saturation	1
ADF	Beta decay factor	0
RSP	Rill spacing (m)	1
SPACING	Average micro-topographic spacing (m)	1

appropriate to our site conditions. Two parameters that model infiltration processes, capillary drive (G) and  $\alpha$  fitting parameter (ALF) for infiltration calculations, were the only parameters that had a well-defined value or range of values for similarly textured soils in the closely related KINEROS2 model (Smith et al., 1995). With respect to the canopy interception parameter (IN), Dunkerley and Booth (1999) measured rainfall interception by dryland shrubs and grasses with variable cover and rainfall intensity and compared their data with other published data. That study showed a high degree of variability in measurements of rainfall interception, depending on the method used, vegetation type, amount of cover, and rainfall intensity, so we used RHEM's default value of 1 mm for IN. The general input parameters that were not calibrated for both field sites are presented in Table 1.

Parameters relating to soil texture (FRACT) and porosity (POR) were calculated separately for each site based on field data. Several input parameters were directly estimated for each plot using field measurements. Percent cover of plant basal area (C<sub>b</sub>), litter (C<sub>l</sub>), and rock (C<sub>r</sub>) was estimated from the plot orthophotos. Percent vegetation canopy cover (C<sub>vc</sub>) was derived from the vegetation map for each plot. No cryptobiotic crusts were present.

**Table 2**  
RHEM parameters for porosity (POR), texture fractions (FRACT), slope (S), Chezy coefficient (m s<sup>-2</sup>), splash and sheet erosion (K<sub>SS</sub>, unitless), concentrated flow erosion (K<sub>ω</sub>, s<sup>2</sup> m<sup>-2</sup>), infiltration (K<sub>e</sub>, mm h<sup>-1</sup>), and cover fraction of vegetation canopy (C<sub>vc</sub>), rock (C<sub>r</sub>), litter (C<sub>l</sub>), and plant basal area (C<sub>b</sub>).

Site	POR	FRACT	Plot	S	Chezy	K <sub>SS</sub>	K <sub>ω</sub>	K <sub>e</sub>	C <sub>vc</sub>	C <sub>r</sub>	C <sub>l</sub>	C <sub>b</sub>
Price	0.447	Clay	1	0.059	8.628	20,950	0.026	1.469	0.079	0	0.007	0.002
			2	0.048	8.489	17,659	0.025	1.545	0.059	0	0.032	0.003
		Finer silt	3	0.007	9.562	13,263	0.025	1.52	0.109	0	0.02	0.007
			4	0.059	8.315	16,734	0.025	1.556	0.113	0	0.029	0.01
		Coarser silt	5	0.067	8.117	17,111	0.025	1.564	0.119	0	0.032	0.009
			6	0.057	8.416	14,020	0.025	1.582	0.178	0	0.024	0.022
		Fine sand	7	0.066	8.026	17,008	0.024	1.6	0.08	0	0.041	0.011
			8	0.1	7.69	24,628	0.026	1.518	0.072	0.002	0.017	0.01
		Medium sand	9	0.094	7.835	25,142	0.026	1.496	0.064	0.002	0.014	0.005
			10	0.075	8.128	21,748	0.025	1.526	0.049	0.002	0.02	0.009
		11	0.03	9.115	16,894	0.026	1.514	0.057	0.003	0.015	0.01	
Ferron	0.403	Clay	1	0.169	6.213	19,149	0.002	1.75	0.206	0.01	0.045	0.052
			2	0.114	7.194	14,614	0.002	1.728	0.198	0.007	0.036	0.055
		Finer silt	3	0.185	6.186	28,252	0.002	1.607	0.18	0.005	0.026	0.028
			4	0.201	5.928	29,548	0.002	1.631	0.183	0.003	0.03	0.032
		Coarser silt	5	0.214	5.691	24,141	0.002	1.736	0.24	0	0.035	0.058
			6	0.183	5.932	17,289	0.002	1.823	0.242	0	0.056	0.061
		Fine sand	7	0.2	5.985	26,454	0.002	1.65	0.223	0	0.026	0.042
			8	0.187	6.128	24,449	0.002	1.7	0.177	0.002	0.029	0.053
		Medium sand	9	0.245	5.408	36,656	0.002	1.575	0.264	0.003	0.021	0.024
			10	0.206	5.764	26,909	0.002	1.633	0.252	0	0.039	0.023
		11	0.184	6.226	25,663	0.002	1.594	0.243	0	0.025	0.025	
		12	0.19	6.078	28,022	0.002	1.606	0.202	0	0	0.024	

The Chezy coefficient for overland and concentrated flow was estimated using a modified equation by Crowe et al. (2009):

$$Chezy = \sqrt{\frac{8g}{f_t}} \tag{1}$$

where g is the acceleration of gravity (m s<sup>-2</sup>) and f<sub>t</sub> is the Darcy-Weisbach friction factor estimated by Al-Hamdan et al. (2013) as:

$$f_t = 10^{-0.109-1.425C_l+0.442C_r+1.764C_b+2.068S} \tag{2}$$

where C<sub>l</sub> is the fraction of litter cover, C<sub>r</sub> is the fraction of rock cover, C<sub>b</sub> is the fraction of basal area, and S is percent slope.

Per the RHEM documentation, the splash and sheet erosion erodability coefficient, K<sub>SS</sub>, was estimated as:

$$K_{SS} = 10^{4.2587-2.547(C_b+C_l)-0.7822C_{vc}+2.5535S} \text{ if } C_b + C_l \leq 0.475 \tag{3}$$

where C<sub>vc</sub> is the fraction of projected vegetation canopy cover (Table 2). C<sub>b</sub> + C<sub>l</sub> was <0.475 for all plots in both field locations. Note this equation is specifically for estimating splash and sheet erosion of shrub dominated hillslopes. RHEM offers several other K<sub>SS</sub> equations to model splash and sheet erosion processes on hillslopes dominated by other vegetation communities.

The undisturbed concentrated flow erodability coefficient, K<sub>ω</sub>, was calculated following Al-Hamdan et al. (2015) as:

$$K_{\omega} = 10^{-4.14-1.28C_b-0.98C_r-15.16T_c+7.09T_s} \tag{4}$$

where T<sub>c</sub> and T<sub>s</sub> are the clay and silt fractions measured at each site.

The effective hydraulic conductivity (mm h<sup>-1</sup>), K<sub>e</sub>, which characterizes infiltration, was calculated using the following equations (RHEM, 2015a):

$$K_{eb} = 1.2 * \exp^{2.0149(C_b+C_l)} \tag{5}$$

$$K_e = K_{eb} * 1.2 \tag{6}$$

Eq. (5) is specific for silt loam textured soils and the coefficient (1.2) in Eq. (6) is specifically used to estimate K<sub>e</sub> for sites dominated by shrub

vegetation cover. Table 2 shows the plot-varying input parameters. Detailed RHEM input file parameter descriptions can be found at <http://apps.tucson.ars.ag.gov/rhem/docs>.

No prior RHEM calibration data exists for saline and sodic soils like those of the Mancos Shale formation, so a multi-objective optimization method was used to calibrate the model to match simulation results. Calibrations used the multi-objective complex (MOCOM) optimization method of Yapo et al. (1998), a downhill simplex search that uses a controlled random search, competitive evolution, and Pareto ranking. MOCOM calculates a set of Pareto optimal solutions that show the tradeoffs between objective measures, in this case root mean square error (RMSE) and absolute percent bias (%Bias). A solution was selected that had the lowest bias or the second lowest in cases where RMSE improved and there was no substantial increase in bias.

Separate calibrations were calculated for the Price and Ferron sites. First, SAT (initial degree of soil saturation),  $K_e$ , and ALF ( $\alpha$  fitting parameter) were calibrated to match field-measured discharge (mm), and then  $K_{ss}$  and  $K_{co}$  were subsequently calibrated to match field-measured sediment loads (kg). SAT and ALF were calibrated directly from a wide range of values.  $K_e$ ,  $K_{ss}$ , and  $K_{co}$  were calibrated by varying a multiplicative coefficient ( $C_e$ ,  $C_{ss}$ , and  $C_{co}$ ) that was applied to the values calculated in Eqs. (3), (4), and (6).

Performance of the calibrated RHEM was evaluated using residual plots, the coefficient of determination ( $R^2$ ), Nash–Sutcliffe efficiency (NSE) (Nash and Sutcliffe, 1970), and the ratio of root-mean-squared error to standard deviation (RSR) (Legates and McCabe, 1999):

$$NSE = 1 - \frac{\sum_{i=1}^n (O_i - P_i)^2}{\sum_{i=1}^n (O_i - O_{avg})^2} \quad (7)$$

$$RSR = \frac{\sqrt{\sum_{i=1}^n (O_i - P_i)^2}}{\sqrt{\sum_{i=1}^n (O_i - O_{avg})^2}} \quad (8)$$

where  $n$  is the number of plots,  $P_i$  is the predicted value of plot  $i$ ,  $O_i$  is observed, and  $O_{avg}$  is the average of the observed plot values. NSE varies from  $-\infty$  to 1, with 0 indicating that per-sample predictions are no better than simply using the mean and 1.0 indicating perfect correspondence between predicted and observed values. RSR ranges from 0 to  $+\infty$  with higher values indicating the degree of prediction error relative to variability in a particular set of observed values, thereby facilitating the comparison of model results from experiments with differing ranges of observed values.

A sensitivity analysis was performed to determine how  $K_e$ ,  $K_{co}$ , and  $K_{ss}$  affect the discharge and sediment load outputs of the model for each site. Calibrated values of  $K_{ss}$ ,  $K_{co}$ , and  $K_e$  for each plot were each separately varied by 10% increments to  $\pm 50\%$  and the relative change

in discharge and sediment load was plotted. The effect of VCC was tested by running the model with 10% increments in vegetation cover from 0% to 100% and plotting the relative change in mean sediment load output across all plots.

## 2.5. VDSH analysis

VDSH was measured using the landscape pattern metrics available in the Fragstats (v4.2) computer program (McGarigal and Marks, 1995). These metrics can quantify the overall landscape pattern and the specific class level patterns of VCC or soil interspaces. All the available class level metrics were calculated (103 metrics). This included metrics for area-edge (landscape composition/non-spatially explicit landscape configuration), shape (landscape configuration), contrast (difference between patch types), and aggregation (landscape texture). Edge effect options and the search radius of aggregation metrics were set to 1 m and the threshold distance for CONNECT (aggregation metric that describes how connected the patches are) was set to 0.1 m.

Results were analyzed separately for each field site, and for both sites combined.  $R^2$  values were calculated between each class pattern metric and the error residuals of the RHEM sediment load predictions. Histograms were created to examine the distribution of  $R^2$  values and identify which metrics had the highest values. Tests of  $R^2$  values included quadratic and linearized forms of the metrics as well. Among those metrics that had a high  $R^2$ , graphs of each metric versus residuals were examined in relation to the vegetation maps in order to select one representative metric for the pattern of soil interspaces and one for the pattern of vegetation. Error residuals for RHEM sediment load predictions were also regressed against VCC and slope to examine if the relationship of VDSH to model residuals might simply be a spurious correlation to these two influential model parameters.

## 3. Results

### 3.1. RHEM

In multiple attempts at calibrating discharge of the RHEM, Price plot 12 (50 year storm) was a significant outlier (2.87 standard deviations) that unduly affected the Price calibration. This was likely because the simulation was inadvertently run longer than the others, so this plot was excluded from the remainder of the study. Fig. 3 displays plots of the Pareto optimal solutions for the RHEM calibration with the selected solution indicated as a black asterisk. RMSE values for the two field sites are plotted using separate measurement scales on opposing X axes of Fig. 3 since their ranges were each quite narrow and very different from each other. Table 3 shows the allowable ranges of calibration parameters, calibrated values, associated %Bias] and RMSE. Table 4 shows the calibrated  $K_{ss}$ ,  $K_{co}$ , and  $K_e$  values for each field plot.

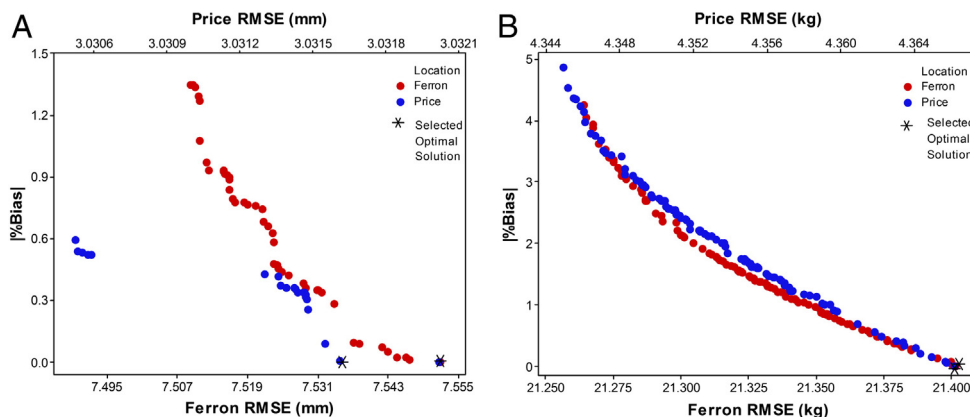


Fig. 3. Price and Ferron Pareto optimal solutions for discharge (A) and sediment load (B).

**Table 3**

Calibrated parameters (unitless) and calibration results for discharge and sediment load: initial soil saturation (SAT), fitting parameter for infiltration (ALF), and scaling coefficients ( $C_e$ ,  $C_{ss}$ , and  $C_{\omega}$ ) for RHEM's  $K_e$ ,  $K_{ss}$ , and  $K_{\omega}$  parameters.

Calibration	Site	Parameter	Calibration range	Calibrated value	[%Bias]	RMSE	
Discharge	Price	SAT	0.04–0.09	0.073	0.006	3.03 mm	
		$C_e$	0.1–10	0.194			
		ALF	0.7–0.95	0.892			
	Ferron	SAT	0.04–0.09	0.085		0.004	7.55 mm
		$C_e$	0.1–10	5.841			
		ALF	0.7–0.95	0.795			
Sediment load	Price	$C_{ss}$	0.1–10	1.788	0.007	4.37 kg	
		$C_{\omega}$	0.1–10	5.301			
		$C_{ss}$	0.1–10	3.139			
	Ferron	$C_{ss}$	0.1–10	3.139		0.02	21.4 kg
		$C_{\omega}$	0.1–10	2.578			
		$C_{\omega}$	0.1–10	2.578			

For discharge, Price and Ferron could both be calibrated to an essentially unbiased solution. Based on the incremental changes in [%Bias] and RMSE, the solution set with the second lowest [%Bias] was selected for Price and the lowest [%Bias] for Ferron (Fig. 3A). Price had an RMSE of 3.03 mm whereas Ferron had a higher RMSE of 7.55 mm (Table 3). Before applying the calibrated  $C_e$  coefficients, the Price  $K_e$  values that were calculated based on the model documentation were slightly lower than Ferron (Table 2) because Ferron contained greater basal and litter cover. However, the calibration resulted in a  $C_e$  for Ferron that was more than an order of magnitude larger than Price (Table 3), greatly magnifying the difference between sites for this parameter.

For sediment load, both sites were also calibrated to an essentially unbiased solution. The solution set with the lowest [%Bias] was selected for Price and the second lowest [%Bias] for Ferron (Fig. 3B). Price had an RMSE of 4.37 kg whereas Ferron had a substantially higher RMSE of 21.4 kg (Table 3). Before applying the calibrated  $C_{ss}$  and  $C_{\omega}$ , the initial  $K_{ss}$  values for Price plots were lower than Ferron while  $K_{\omega}$  for Ferron was an order of magnitude smaller than Price (Table 2). This is because Ferron had greater slope (greatest weighting in Eq. (3)), VCC, basal cover, and soil clay fraction (greatest weighting in Eq. (4)). After calibration,  $C_{ss}$  for Price was about half that of Ferron and  $C_{\omega}$  at Ferron was about half that of Price, magnifying the difference between sites for these two parameters.

Table 5 shows the model performance using several metrics. While the RMSE for Ferron discharge and sediment load calibrations was greater than Price (Table 3), the RSR for both sites were similar (Table 5). All three performance metrics indicate that RHEM estimated discharge better at Price, but sediment load better at Ferron. At Price, the plot of residuals for sediment load estimates (Fig. 4) shows that while RHEM calibrated to the overall site mean, it did a poor job of reproducing the range of variability between plots. Low observed values were overpredicted, and high observations were underpredicted. A similar, less pronounced pattern occurred with the Price discharge estimates as well. In contrast, Ferron discharge and sediment load residuals possessed a random pattern. Overall, RHEM modeled discharge and sediment load erosion processes at Ferron better than Price.

**Table 4**

Calibrated RHEM parameters for splash and sheet erosion ( $K_{ss}$ ), concentrated flow erosion ( $K_{\omega}$ ), and infiltration ( $K_e$ ).

Site	Parameter	Plot											
		1	2	3	4	5	6	7	8	9	10	11	12
Price	$K_{ss}$	37,458	31,575	23,714	29,920	30,594	25,068	30,411	44,035	44,954	38,886	30,206	–
	$K_{\omega}$	0.14	0.13	0.135	0.131	0.13	0.133	0.127	0.136	0.137	0.134	0.136	–
	$K_e$	0.285	0.3	0.295	0.302	0.303	0.307	0.31	0.295	0.29	0.296	0.294	–
Ferron	$K_{ss}$	60,109	45,874	88,683	92,752	75,779	54,270	83,038	76,746	115,064	84,467	80,557	87,960
	$K_{\omega}$	0.004	0.004	0.004	0.004	0.004	0.004	0.004	0.004	0.004	0.004	0.004	0.004
	$K_e$	10.222	10.093	9.385	9.525	10.137	10.648	9.635	9.929	9.2	9.537	9.309	9.38

**Table 5**

Model performance results.

Location	Discharge/sediment load	R <sup>2</sup>	NSE	RSR
Price	Discharge	0.918	0.898	0.307
Ferron	Discharge	0.798	0.777	0.420
Price	Sediment load	0.510	0.509	0.643
Ferron	Sediment load	0.642	0.627	0.543

Fig. 5 shows how RHEM discharge and sediment load outputs respond to changes in  $K_{ss}$ ,  $K_{\omega}$ , and  $K_e$  at each site. For  $K_{ss}$ , Price and Ferron have a comparable change in sediment (Price: +46%, –35%; Ferron: +46%, –42%). Changes in  $K_{\omega}$  have practically no effect at Price and only a small effect at Ferron (+1%, –1%). The Ferron site is more responsive to  $K_e$  (Sediment load: +17%, –13%; Discharge: +25%, –17%) than Price is (Sediment load: +4%, –3%; Discharge: +6%, –4%).

Fig. 6 shows how changes in VCC affect the RHEM discharge and sediment load outputs for each site. As expected, increasing VCC results in less modeled discharge and sediment load at each site. Modeled sediment loading had a greater response at Ferron (+123%, –95%) than at Price (+36%, –64%). For Price, as VCC exceeds 30% the marginal decrease in sediment load from adding more vegetation is small and fairly constant. For Ferron, the marginal decrease in sediment loading does not level off until almost 100% cover. Ferron showed a much greater response to discharge (+6%, –68%) than Price (+1%, –21%). The best fit linear exponential equations were calculated and presented below:

$$\begin{aligned}
 \text{DryXDischarge} &= -0.7463x + 1.074, R^2 = 0.99 \\
 \text{PriceDischarge} &= -0.2166x + 1.016, R^2 = 0.99 \\
 \text{DryXSediment} &= 2.202e^{-3.94x} + 1.074, R^2 = 0.99 \\
 \text{PriceSediment} &= 1.172e^{-1.62x} + 1.016, R^2 = 0.99
 \end{aligned}$$

where  $x$  is percent foliar cover.

### 3.2. Vegetation spatial distribution

In order to assess the most broadly applicable metric, we selected the metric that worked best at Price and Ferron (Both) rather than focusing on each site individually (Table 6). The class metric for the spatial pattern of the soil interspaces that had the strongest  $R^2$  was the coefficient of variation of the fractal dimension index (FRAC\_CV, Fig. 7). FRAC\_CV is a shape metric that describes the variability of complexity in the shape of objects (McGarigal and Marks, 1995). Plots with high variability in shape complexity (e.g. tortuosity) of the interspace area, produced less sediment loading than the model predicted.

When applying Fragstats to the pattern of vegetation cover, the metric with the best  $R^2$  value was GYRATE\_MD. GYRATE\_MD is the median value of the radii required to perfectly encircle each individual patch of vegetation in the map. However, on examination of the relationship to residuals and the plot maps, we judged the relationship to be an artifact of using the median of polygon shape values. Some of the plot maps

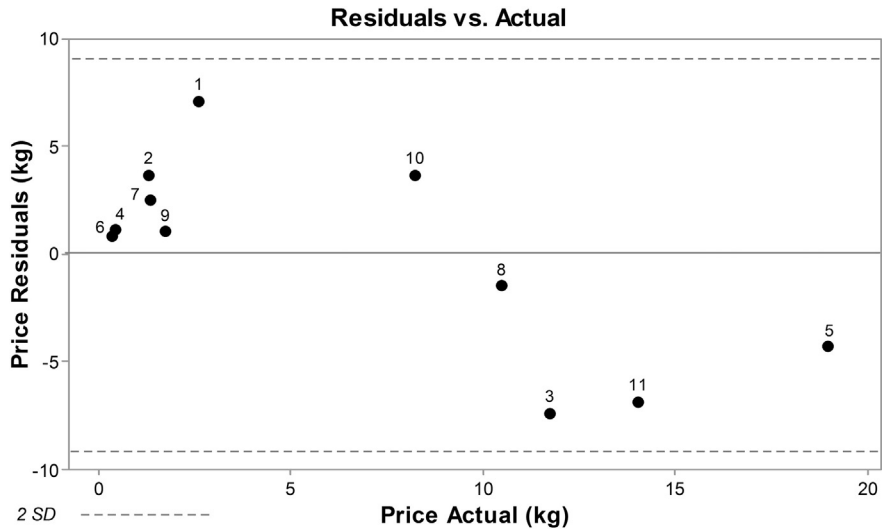


Fig. 4. Residual plot for Price sediment load model output.

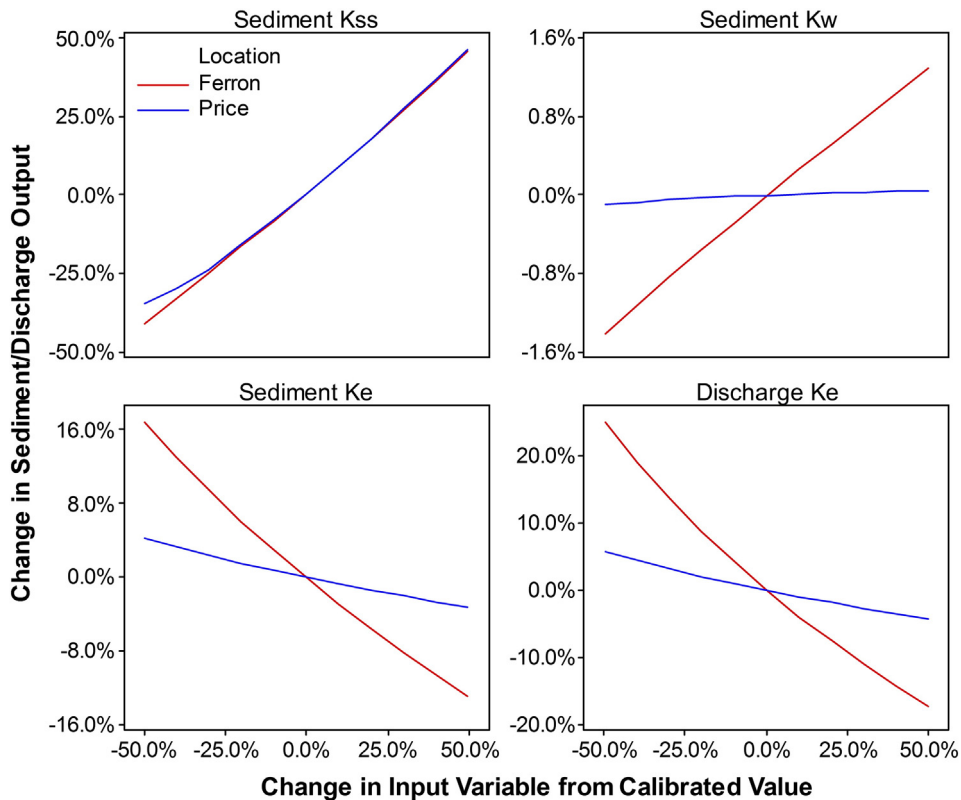


Fig. 5. Sensitivity of change in  $K_{ss}$ ,  $K_w$ , and  $K_e$  on sediment load and  $K_e$  on discharge output.

included a few very large patches of vegetation and many tiny patches. Use of the median disregarded important information about the extremes. Disregarding the medians, the next strongest relationship was the coefficient of variation of the contiguity index (CONTIG\_CV, Fig. 8). CONTIG\_CV is a measure of the variability of patch contiguity and shape (McGarigal, 2015). Plots with high patch contiguity of vegetation area produced less sediment loading than the model predicted.

The vegetation maps in Fig. 9 show how the FRAC\_CV and CONTIG\_CV metrics differentiate plots that have similar amounts of VCC but different spatial patterns. For the two plots with high VCC

(Fig. 9A,B), the more complex spatial distribution (Fig. 9B) has a higher FRAC\_CV (101.1 > 10.2) and CONTIG\_CV (115.6 > 87.7). A similar differentiation by FRAC\_CV (22.4 > 11.2) and CONTIG\_CV (100.8 > 93.9) is seen in two plots with low VCC (Fig. 9C,D).

#### 4. Discussion

A number of studies have successfully calibrated RHEM (discharge and sediment load) for variable VCC and slope on burned, disturbed, and undisturbed plots (Al-Hamdan et al., 2012, 2015; Felegari et al.,

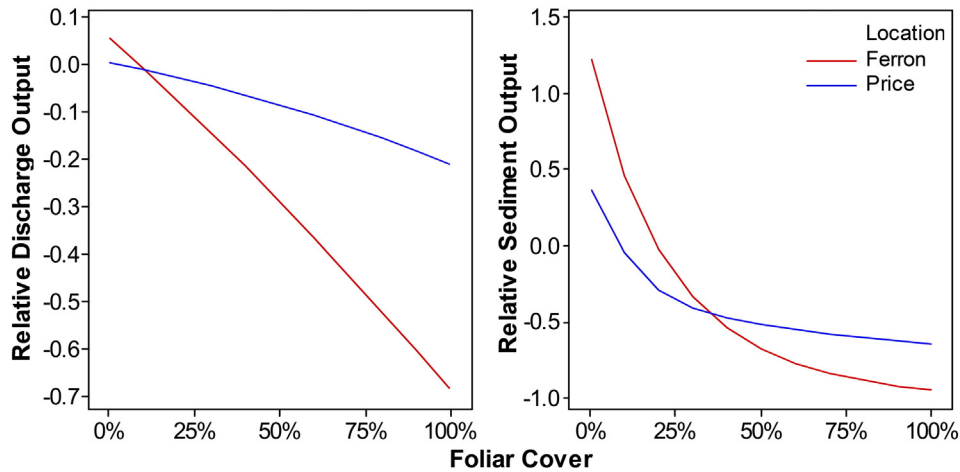


Fig. 6. Sensitivity of change in foliar cover on discharge and sediment load output.

2014; Hernandez et al., 2013; Zhang et al., 2012, Nearing et al., 2011). These results extend that knowledge base to saline and sodic soils of the Mancos Shale. Three of the RHEM parameters relate the amount of vegetation to discharge and erosion processes:  $K_e$  (infiltration),  $K_{ss}$  (splash and sheet erosion), and  $K_{co}$  (concentrated flow erosion). Our results show that for saline and sodic soils of the Mancos Shale formation, the calibrated  $K_e$  values at Price (Table 4) were lower than initially calculated from Eq. (5) for silt-loams and were higher at Ferron. In addition,  $K_e$  values for shrub dominated communities reported by Zhang et al. (2012) were an order of magnitude greater than the Price calibrated values, but half of the Ferron calibrated values. Calibrated  $K_{ss}$  values from both sites were an order of magnitude greater than values reported for Castlehead burned plots in Al-Hamdan et al. (2015) and an order of magnitude lesser than the values reported by Zhang et al. (2012).  $K_{co}$  values from Ferron were comparable to values reported in Al-Hamdan et al. (2015) and an order of magnitude greater than Upper Sheep low sagebrush unburned/burned plot values reported in Al-Hamdan et al. (2012). Price  $K_{co}$  values were up to three orders of magnitude greater on these highly erodible soils than the values reported in both papers.

Infiltration rates are affected by soil surface conditions (Branson et al., 1981), including vegetation (Lyford and Qashu, 1969; Thompson et al., 2010) and slope (Nassif and Wilson, 1975; Fox et al., 1997; Mu et al., 2015). Fig. 10 shows the average time-varying infiltration rates from the 10-year storm simulations at each site. Despite having lower slope values, the infiltration rate at Price started lower than Ferron ( $81.7 \text{ mm h}^{-1}$  versus  $113.2 \text{ mm h}^{-1}$ ), decreased more rapidly over time, and stabilized at a lower rate ( $11.6 \text{ mm h}^{-1}$  versus  $17.1 \text{ mm h}^{-1}$ ). These differences in infiltration rates are consistent with the original plot values for RHEM’s hydraulic conductivity parameter ( $K_e$ ) which were almost always greater at Ferron (Table 2) due to larger amount of plant litter and basal area (Eq. (5)). However, the substantial difference in  $C_e$ , the calibrated scaling coefficient for  $K_e$ , indicates that the default values of 1.2 in Eq. (5) based on soil texture and also 1.2 in Eq. (6) based on a shrub life form would have resulted in biased predictions of infiltration and discharge.

RHEM predictions of discharge for Price were better than Ferron, as indicated by a higher  $R^2$  and NSE and a lower RSR (Table 5). Despite this, RHEM’s error residuals for sediment load at Price did not capture the

plot-to-plot variability as well as at Ferron (Fig. 4, Table 5). The disparity may be related to the low VCC resulting in a higher potential for splash and sheet erosion, low slope resulting in lower discharge velocity, and even the soil crusts found at Price that may influence infiltration. Another possibility may be related to how RHEM estimates rill width (RSP) and rill average micro-topographic spacing (SPACING). In this study, we set both parameters as 1 m for both sites which may not accurately represent each site.

It is important to note that in our RHEM simulations, a 1 m rill spacing was used. The value of 1 m rill spacing was a reasonable default approximation of rangeland rill spacing derived from experimental research on cropland (Gilley et al., 1990). This value is currently used as a default rill spacing in RHEM when no specific data is available. A 1 m rill spacing in our experiment assumes that only one concentrated flow channel was formed in the middle of our experimental 2-m-wide plot. Rill spacing at Price and Ferron are most likely different, and may be significantly different from 1 m. Concentrated flow estimation at both sites was therefore influenced by the 1 m rill spacing assumption. Nevertheless, it is difficult to assess the magnitude of this influence without data appropriately collected to quantify the actual spatial extent of concentrated flow networks at both sites. Perhaps the use of three-dimensional reconstruction can be helpful in helping clarify the link between VCC and the spatial distribution of concentrated flow networks.

Table 6  
 $R^2$ s for linear regressions of selected spatial pattern metrics versus RHEM sediment load error residuals.

Metric	Location	$R^2$	p-Value	Name	Type
Class - Soil	Both	0.46	<0.001	FRAC_CV	Shape
Class - Veg	Both	0.33	0.004	CONTIG_CV	Shape

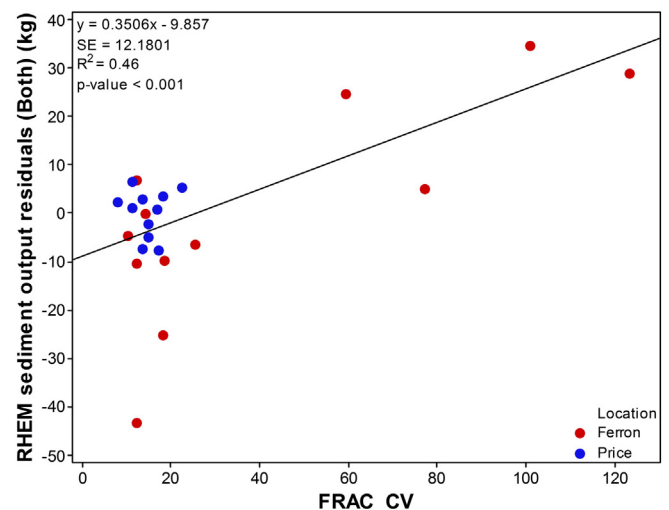


Fig. 7. Linear regression of FRAC\_CV vs. RHEM sediment load error residuals at Price and Ferron combined (Both).

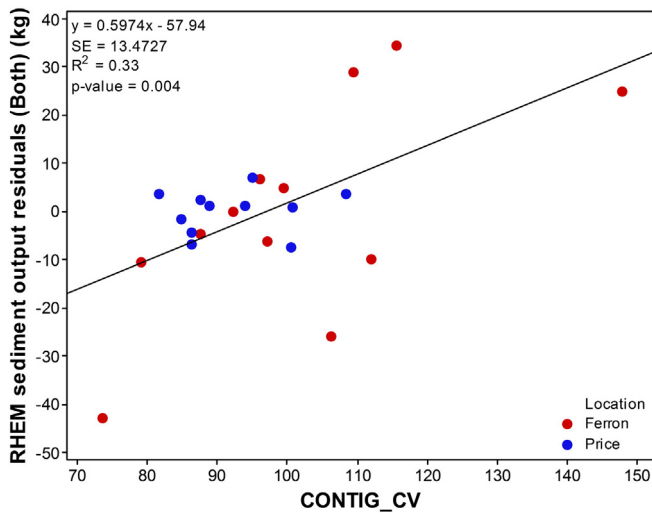


Fig. 8. Linear regression of CONTIG\_CV vs. RHEM sediment load error residuals at Price and Ferron combined (Both).

The most sensitive sediment erosion parameter was  $K_{ss}$  (Fig. 5). Both sites showed relatively proportional change to each other. This indicates VCC and slope have a proportional effect on splash and sheet erosion. In addition, Table 4 shows that  $K_{ss}$  values are higher at Ferron than Price. Infiltration ( $K_e$ ) and concentrated flow erosion ( $K_{co}$ ) were less sensitive than  $K_{ss}$  and in each case, Ferron showed greater change than Price for these parameters. This result indicates that VCC has little effect on simulated concentrated flow erosion and infiltration at Price, but it has more effect at a site with greater VCC and slope like Ferron.

RHEM predicts Ferron to be more sensitive to changes in vegetation cover than Price (Fig. 6), probably because of the greater slopes. As the

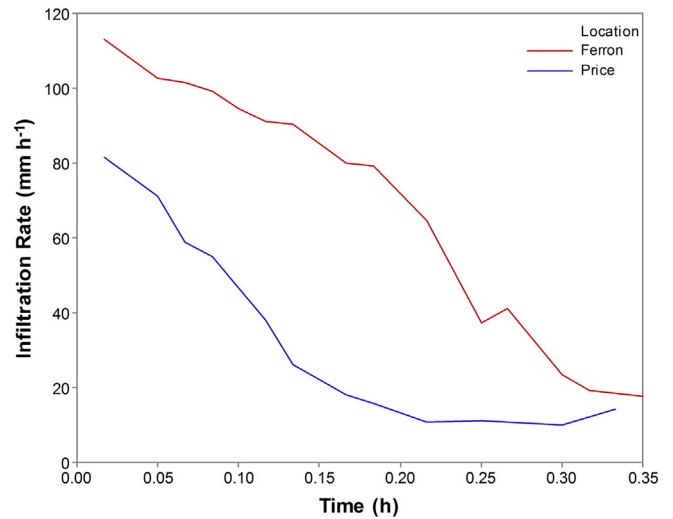


Fig. 10. Site-averaged infiltration rates since start of runoff for 10-year storm simulations at Price and Ferron.

VCC input for RHEM approaches 100%, the modeled sediment load output reaches a low marginal reduction in sediment load output. This result contrasts with Bartley et al. (2006) who found that even with high mean VCC, hillslopes with small patches of interspace had substantially more runoff and sediment load than similar hillslopes with fewer or no interspace patches. This disagreement and the degree of extrapolation beyond the range of conditions used in RHEM's calibration means that the estimate of up to 95% reduction in sediment load output at 100% VCC should be regarded with great caution. However, the environmental conditions in Bartley et al. (2006) (tropical semi-arid savanna rangelands) were different from Price and Ferron, and it is unlikely

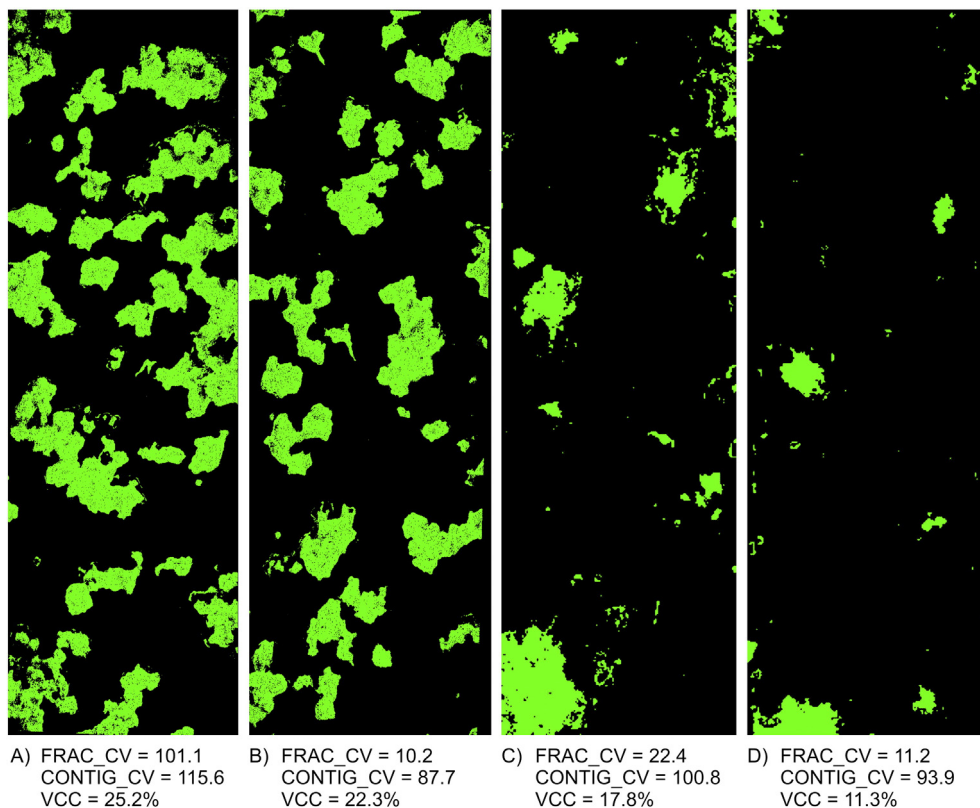


Fig. 9. Maps showing the spatial distribution of vegetation (green) relative to soil (black) for (A) Ferron plot 10, (B) Ferron plot 7, (C) Price plot 6, and (D) Price plot 4. (For interpretation of the references to colour in this figure legend, the reader is referred to the web version of this article.)

that a cover of 100% could ever be established in the arid, saline environment of the Mancos Shale.

Puigdefabregas (2005) suggests that VDSH explains the relationship between soil development and evolution processes and in turn, influences sheet and concentrated flow processes (Wilcox et al., 1996; Davenport et al., 1998; Urgeghe et al., 2010). Furthermore, VDSH may affect the amount of runoff and infiltration (Chartier et al., 2011). Our results indicate that spatial pattern metrics that describe VDSH are significantly correlated with the error residuals of sediment load output from RHEM (Table 6) for plots covering a range of VCC (3.3%–26.4%), slope (0.7%–24.5%), and rainfall intensity. RHEM's overprediction of sediment loading for sites with a high FRAC\_CV (Figs. 7 and 9) suggests that tortuous flow paths may be slowing flow and trapping sediment in a way that is not characterized in the model. Fig. 7 shows a non-linear or threshold response where only the highest values of FRAC\_CV drive the regression. This effect is similar in the CONTIG\_CV metric for the pattern of vegetation cover, where sediment loading was less than the model predicted when there was high variability in the contiguity of vegetation patches (Figs. 8 and 9).

VCC is only weakly correlated to FRAC\_CV ( $r = 0.44$ ) and CONTIG\_CV ( $r = 0.49$ ). Regressions of VCC and slope versus the RHEM sediment load error residuals (Fig. 11) show that these two parameters do not have the same type of relationship to the RHEM sediment load residuals that VDSH did. Even though VCC and VDSH are not entirely independent, the regression of VCC to sediment load residuals has a weak  $R^2$  (Slope  $R^2 < 0.01$ , VCC  $R^2 = 0.02$ ) and is statistically insignificant (Fig. 11). The effect of VDSH is not seen as a coincidental relationship to the amount of vegetation cover or slope of the plots.

These results suggest that there may be some benefit to incorporating VDSH into RHEM, but one must proceed with caution when selecting a landscape pattern description. In this case we found that metrics that took the median of patch values may disregard important variability at the extremes and result in spurious relationships. The selected metrics of spatial pattern may reflect how VDSH affects the development of channel networks. Hillslopes with low VCC tend to have runoff concentrate in narrow channels, whereas when VCC becomes

dense, concentrated flow channels widen and decrease the potential for concentrated flow erosion (Puigdefabregas, 2005; Al-Hamdan et al., 2012; Wilcox et al., 1996; Davenport et al., 1998; Urgeghe et al., 2010). In addition, VDSH may also affect the amount of infiltration (Loch, 2000; Chartier et al., 2011).

## 5. Conclusion

This study provides new parameterizations for applying RHEM to saline and sodic soils in rangelands of the Mancos Shale formation to estimate discharge and erosion processes. Calibrated  $K_{ss}$  and  $K_{cs}$  values are generally greater than values reported in previous studies from less saline environments. RHEM did a better job of expressing the plot level variability at the site with steeper slopes and a greater amount of vegetation. Our results show that RHEM simulates discharge (Price  $R^2 = 0.92$ ; Ferron  $R^2 = 0.8$ ) and erosion processes (Price  $R^2 = 0.51$ ; Ferron  $R^2 = 0.64$ ) well on saline and sodic soils of the Mancos Shale formation despite the fact RHEM is not specifically designed to account for soil salinity.

Landscape pattern descriptions showed that when vegetation patches have a variety of contiguous relationships (CONTIG\_CV) and the tortuosity of soil interspaces (FRAC\_CV) reaches high levels, observed sediment loading decreases relative to modeled expectations. These results reinforce prior literature indicating that the spatial distribution of vegetation cover has an impact on sediment erosion processes. Remote sensing has been used to characterize patterns of vegetation and clearings (Frohn et al., 1996), and developers of erosion models like RHEM might consider incorporating the effect of vegetation dependent spatial heterogeneity. Lastly, these findings may help provide land managers valuable data to control sediment erosion processes and contributions to the Colorado River from the Mancos Shale formation.

## Acknowledgements

Funding for this study was provided by the US DOI Bureau of Reclamation/Bureau of Land Management, USDA Agricultural Research

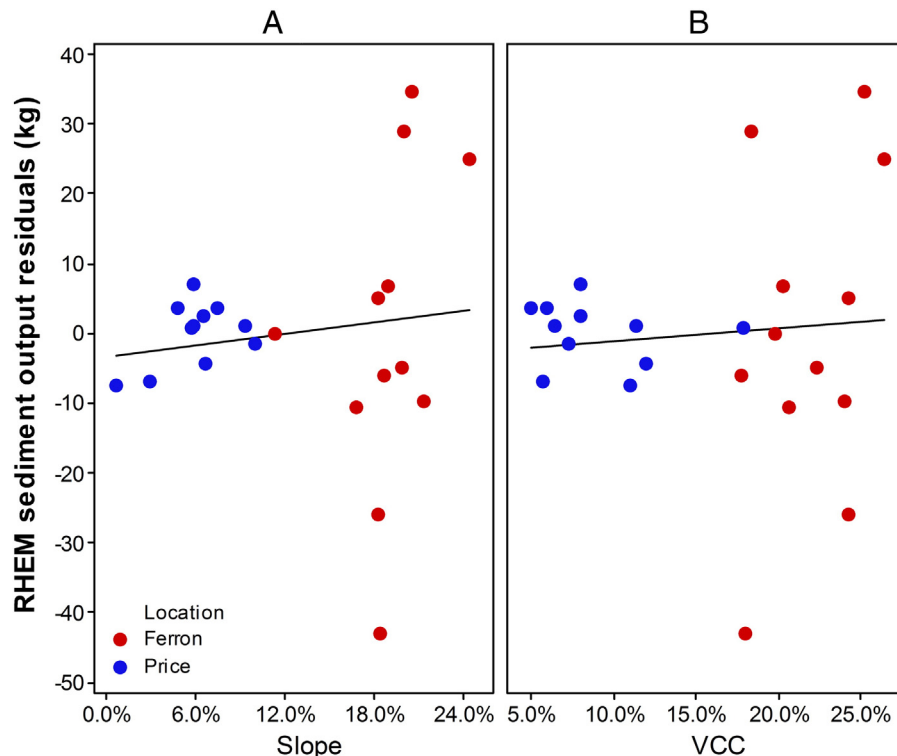


Fig. 11. Regression of RHEM sediment load error residuals versus slope (A) and VCC (B) for both sites.

Service (Cooperative Agreement 59-5370-3-001), and the Desert Research Institute of the Nevada System of Higher Education.

## Appendix A. Supplementary data

Supplementary data associated with this article can be found in the online version, at <http://dx.doi.org/10.1016/j.catena.2016.06.043>. These data include Google map of the most important areas described in this article.

## References

- Al-Hamdan, O.Z., Pierson, F.B., Nearing, M.A., Williams, C.J., Stone, J.J., Kormos, P.R., Boll, J., Weltz, M.A., 2012. Concentrated flow erodability for physically based erosion models: temporal variability in disturbed and undisturbed rangelands. *Water Resour. Res.* 48 <http://dx.doi.org/10.1029/2011wr011464>.
- Al-Hamdan, O.Z., Pierson, F.B., Nearing, M.A., Williams, C.J., Stone, J.J., Kormos, P.R., Boll, J., Weltz, M.A., 2013. Risk assessment of erosion from concentrated flow on rangelands using overland flow distribution and shear stress partitioning. *Transactions of the Am. Soc. Agric. Biol. Eng.* 56 (2), 539–548.
- Al-Hamdan, O.Z., Hernandez, M., Pierson, F.B., Nearing, M.A., Williams, C.J., Stone, J.J., Boll, J., Weltz, M.A., 2015. Rangeland hydrology and erosion model (RHEM) enhancements for applications on disturbed rangelands. *Hydrol. Process.* <http://dx.doi.org/10.1002/hyp.10167>.
- Bartley, R., Roth, C.H., Ludwig, J., McJannet, D., Liedloff, A., Corfield, J., Hawdon, A., Abbott, B., 2006. Runoff and erosion from Australia's tropical semi-arid rangelands: influence of ground cover for differing space and time scales. *Hydrol. Process.* 20 (15), 3317–3333.
- Branson, F.A., Gifford, F.G., Renard, K.G., Hadley, R.F., 1981. *Rangeland Hydrology*. second ed. Soc. for Rangeland Management (84 pp.).
- Carroll, C., Merton, L., Burger, P., 2000. Impact of vegetative cover and slope on runoff, erosion, and water quality for field plots on a range of soil and spoil materials on Central Queensland coal mines. *Soil Res.* 38 (2), 313–328.
- Chartier, M.P., Rostagno, C.M., Pazos, G.E., 2011. Effects of soil degradation on infiltration rates in grazed semiarid rangelands of northeastern Patagonia, Argentina. *J. Arid Environ.* 75 (7), 656–661.
- Crowe, C.T., Elger, D.F., Williams, B.C., Roberson, J.A., 2009. *Engineering Fluid Mechanics*. ninth ed. John Wiley and Sons, Jefferson City.
- Davenport, D.W., Breshears, D.D., Wilcox, B.P., Allen, C.D., 1998. Viewpoint: sustainability of pinon-juniper ecosystems: a unifying perspective of soil erosion thresholds. *J. Range Manag.* 51, 231–240.
- Dunkerley, D.L., Booth, T.L., 1999. Plant canopy interception of rainfall and its significance in a banded landscape, arid western New South Wales, Australia. *Water Resour. Res.* 35 (5), 1581–1586. <http://dx.doi.org/10.1029/1999WR900003>.
- Evangelou, V.P., Whittig, L.D., Tanji, K.K., 1984. Dissolved mineral salts derived from Mancos shale. *J. Environ. Qual.* 13, 146–150.
- Felegari, M., Talebi, A., Dastorani, M.T., Rangavar, A.S., 2014. Efficiency assessment of rangeland hydrology and erosion model (RHEM) for water erosion quantification (case study: Sangane watershed-Iran). *Int. J. Environ. Resour. Res.* 2 (2), 134–146.
- Foster, G.R., 1982. Modeling the erosion process. Chapter 8 in: hydrologic modeling of small watersheds. In: Haan, C.T., Johnson, H.P., Brakensiek, D.L. (Eds.), *ASAE Monograph No. 5*. Am. Soc. of Agric. Eng., St. Joseph, MI, pp. 297–360.
- Fox, D.M., Bryan, R.B., Price, A.G., 1997. The influence of slope angle on final infiltration rate for interrill conditions. *Geoderma* 80, 181–194.
- Frohn, R., McGwire, K., Estes, J., Dale, V., 1996. Using satellite remote sensing analysis to evaluate a socioeconomic and ecological model of land-use change in Rondônia, Brazil. *Int. J. Remote Sens.* 17 (16), 3233–3255.
- Gilley, J.E., Kottwitz, E.R., Simanton, J.R., 1990. Hydraulic characteristics of rills. *Trans. ASAE* 33 (6), 1900–1906.
- Hernandez, M., Nearing, M.A., Stone, J.J., Pierson, F.B., Wei, H., Spaeth, K.E., Heilman, P., Weltz, M.A., Goodrich, D.C., 2013. Application of a rangeland soil erosion model using national resources inventory data in southeastern Arizona (research section). *J. Soil Water Conserv.* 68 (6), 512.
- Howes, D.A., Abrahams, A.D., 2003. Modeling runoff and runoff in a desert shrubland ecosystem, Jornada Basin, New Mexico. *Geomorphology* 53, 45–73.
- Jackson, M.L., Barak, P., 2005. *Soil Chemical Analysis: Advanced Course*. UW-Madison Libraries Parallel Press.
- Jury, W.A., Horton, R., 2004. *Soil Physics*. John Wiley and Sons.
- Legates, D.R., McCabe, G.J., 1999. Evaluating the use of “goodness-of-fit” measures in hydrologic and hydroclimatic model validation. *Water Resour. Res.* 35 (1), 233. <http://dx.doi.org/10.1029/1998WR900018>.
- Loch, R.J., 2000. Effects of vegetation cover on runoff and erosion under simulated rain and overland flow on a rehabilitated site on the Meandu Mine, Tarong, Queensland. *Soil Res.* 38 (2), 299–312.
- Lyford, F.P., Qashu, H.K., 1969. Infiltration rates as affected by desert vegetation. *Water Resour. Res.* 5 (6), 1373–1376.
- McGarigal, K., 2015. FRAGSTATS Help. University of Massachusetts, Amherst.
- McGarigal, K., Marks, B.J., 1995. Spatial pattern analysis program for quantifying landscape structure. Gen. Tech. Rep. PNW-GTR-351. US Department of Agriculture, Forest Service, Pacific Northwest Research Station.
- Mu, W., Yu, F., Li, C., Xie, Y., Tian, J., Liu, J., Zhao, N., 2015. Effects of rainfall intensity and slope gradient on runoff and soil moisture content on different growing stages of spring maize. *Water* 7, 2990–3008.
- Nash, J., Sutcliffe, J.V., 1970. River flow forecasting through conceptual models part I—a discussion of principles. *J. Hydrol.* 10 (3), 282–290.
- Nassif, S.H., Wilson, E.M., 1975. The influence of slope and rain intensity on runoff and infiltration. *Hydrol. Sci.* 20, 539–553.
- Nearing, M.A., Wei, H., Stone, J.J., Pierson, F.B., Spaeth, K.E., Weltz, M.A., Flanagan, D.C., Hernandez, M., 2011. A rangeland hydrology and erosion model. *ASABE* 54 (3), 901–908.
- Nouwakpo, S.K., Weltz, M.A., McGwire, K., 2015. Assessing the performance of structure-from-motion photogrammetry and terrestrial LiDAR for reconstructing soil surface microtopography of naturally vegetated plots. *Earth Surf. Process. Landf.* <http://dx.doi.org/10.1002/esp.3787>.
- Paige, G.B., Stone, J.J., Smith, J.R., Kennedy, J.R., 2004. The Walnut Gulch rainfall simulator: a computer-controlled variable intensity rainfall simulator. *Am. Soc. Agric. Eng.* 20 (1), 25–31.
- Puigdefabregas, J., 2005. The role of vegetation patterns in structuring runoff and sediment fluxes in drylands. *Earth Surf. Process. Landf.* 30, 133–147. <http://dx.doi.org/10.1002/esp.1181>.
- Rao, B.K., Bowles, D.S., Wagenet, R.J., 1984. Salt efflorescence in Price River basin. *J. Environ. Eng.* 110 (2), 457–471.
- Rasely, R.C., Roberts, T.C., Pyper, G.P., 1991. Upper Colorado River Basin rangeland salinity control project. Watershed Resource Condition Evaluation, Phase II Interagency Team Report. Department of Agriculture, Natural Resource Conservation Service, Salt Lake City, Utah, U.S.
- RHEM, 2015a. RHEM parameter estimation equations. <http://apps.tucson.ars.ag.gov/rhem/docs>.
- Simanton, J.R., Weltz, M.A., Larsen, H.D., 1991. Rangeland experiments to parameterize the water erosion prediction project model: vegetation canopy cover effects. *J. Range Manag.* 44 (3), 276–282.
- Smith, R.E., Goodrich, D.C., Woolhiser, D.A., Unkrich, C.L., 1995. Chapter 20: KINEROS: a kinematic runoff and erosion model. In: Singh, V.J. (Ed.), *Computer Models of Watershed Hydrology*, 697–732. Water Resour. Publications, Highlands Ranch, CO.
- Thompson, S.E., Harman, C.J., Heine, P., Katul, G.G., 2010. Vegetation-infiltration relationships across climatic and soil type gradients. *J. Geophys. Res.* 115, G02023. <http://dx.doi.org/10.1029/2009JG001134>.
- Tuttle, M.L.W., Fahy, J.W., Elliott, J.G., Grauch, R.I., Stillings, L.L., 2014a. Contaminants from cretaceous black shale: I. Natural weathering processes controlling contaminant cycling in Mancos shale, southwestern United States, with emphasis on salinity and selenium. *Appl. Geochem.* 46, 57–71. <http://dx.doi.org/10.1016/j.apgeochem.2013.12.010>.
- Tuttle, M.L.W., Fahy, J.W., Elliott, J.G., Grauch, R.I., Stillings, L.L., 2014b. Contaminants from cretaceous black shale: II. Effect of geology, weathering, climate, and land use on salinity and selenium cycling, Mancos shale landscapes, southwestern United States. *Appl. Geochem.* 46, 72–84. <http://dx.doi.org/10.1016/j.apgeochem.2013.12.011>.
- United States Bureau of Reclamation (USBOR), 2005. Quality of water. Colorado River Basin, Progress Report No. 22 (<http://www.usbr.gov/uc/progact/salinity/pdfs/PR22.pdf>).
- United States Department of Agriculture – Natural Resources Conservation Service, 2013s. Web soil survey national cooperative soil survey. [https://soilseries.sc.egov.usda.gov/OSD\\_Docs/P/PERSAYO.html](https://soilseries.sc.egov.usda.gov/OSD_Docs/P/PERSAYO.html).
- United States Department of Agriculture – Natural Resources Conservation Service, 2013s. Web soil survey national cooperative soil survey. [https://soilseries.sc.egov.usda.gov/OSD\\_Docs/C/CHIPETA.html](https://soilseries.sc.egov.usda.gov/OSD_Docs/C/CHIPETA.html).
- Urgeghe, A.M., Breshears, D.D., Martens, S.N., Beeson, P.C., 2010. Redistribution of runoff among vegetation patch types: on ecophysiological optimality of herbaceous capture of run-on. *Rangel. Ecol. Manag.* 63, 497–504.
- Wei, H., Nearing, M.A., Stone, J.J., Guertin, D.P., Spaeth, K.E., Pierson, F.B., Nichols, M.H., Moffett, C.A., 2009. A new splash and sheet erosion equation for rangelands. *Soil Sci. Soc. Am. J.* 73 (4), 1386–1392.
- Wilcox, B., Davenport, D., Pitlick, J., Allen, C., 1996. *Runoff and Erosion from a Rapidly Eroding Pinyon-Juniper Hillslope*. Los Alamos Natl. Lab, NM (United States).
- Wischmeier, W.H., 1911, Smith, D.D., 1905, United States. Science and Education Administration, and Purdue University. Agricultural Experiment Station, 1978. *Predicting Rainfall Erosion Losses: A Guide to Conservation Planning*. (No. 537.). Washington: Dept. of Agriculture, Science and Education Administration: for sale by the Supt. of Docs., U.S. Gov. Print. Off.
- Wood, M.K., Jones, T.L., Vera-Cruz, M.T., 1998. Rainfall interception by selected plants in the Chihuahuan Desert. *J. Range Manag.* 91–96.
- Yapo, P.O., Gupta, H.V., Sorooshian, S., 1998. Multi-objective global optimization for hydrologic models. *J. Hydrol.* 204, 83–97.
- Zhang, Y., Hernandez, M., Anson, E., Nearing, M.A., Wei, H., Stone, J.J., Heilman, P., 2012. Modeling climate change effects on runoff and soil erosion in southeastern Arizona rangelands and implications for mitigation with conservation practices. *J. Soil Water Conserv.* 67 (5), 390–405.
- Zucca, C., Julitta, F., Previtali, F., 2011. Land restoration by fodder shrubs in a semi-arid agro-pastoral area of Morocco. Effects on soils. *Catena* 87 (3), 306–312.